On planet formation in HL Tau

Giovanni Dipierro[1,2]⋆, Daniel Price[1]†, Guillaume Laibe[3], Kieran Hirsh[1], Alice Cerioli[2] and Giuseppe Lodato[2]

[1]*Monash Centre for Astrophysics (MoCA) and School of Physics and Astronomy, Monash University, Clayton Vic 3800, Australia*
[2]*Dipartimento di Fisica, Università Degli Studi di Milano, Via Celoria, 16, Milano, I-20133, Italy*
[3]*School of Physics and Astronomy, University of St. Andrews, North Haugh, St. Andrews, Fife KY16 9SS, UK*

ABSTRACT

We explain the axisymmetric gaps seen in recent long-baseline observations of the HL Tau protoplanetary disc with the Atacama Large Millimetre/Submillimetre Array (ALMA) as being due to the different response of gas and dust to embedded planets in protoplanetary discs. We perform global, three dimensional dusty smoothed particle hydrodynamics calculations of multiple planets embedded in dust/gas discs which successfully reproduce most of the structures seen in the ALMA image. We find a best match to the observations using three embedded planets with masses of 0.2, 0.27 and 0.55 $M_{\rm J}$ in the three main gaps observed by ALMA, though there remain uncertainties in the exact planet masses from the disc model.

Key words: protoplanetary discs — planet-disc interactions — dust, extinction — submillimetre: planetary systems

1 INTRODUCTION

Recent long-baseline observations of the HL Tau protoplanetary disc at mm to cm wavelengths using the Atacama Large Millimetre/Submillimetre Array (ALMA) revealed a striking series of concentric, axisymmetric gaps, thought to indicate the presence of massive protoplanetary bodies caught in the act of forming planets (ALMA Partnership 2015).

While gap carving by planets embedded in discs has been predicted theoretically since at least Lin & Papaloizou (1986), the axisymmetry of the rings in HL Tau is puzzling. First, prominent spiral waves induced by the planet are seen in all theoretical simulations of planets carving gaps in gas discs whenever the planet is massive enough to open a gap (e.g. de Val-Borro et al. 2006). Second, prior observational estimates of the relative disc mass in HL Tau suggested a disc of 0.03–0.14 $M_{\odot}$ around a 0.5-1.3 $M_{\odot}$ star (e.g. Robitaille et al. 2007; Kwon et al. 2011, 2015; the latter authors estimated ≈ 0.1 $M_{\odot}$ based on fitting disc models to the previous best observations at mm wavelengths). Massive discs should almost certainly show gravitationally instability and hence prominent and large scale spiral arms (e.g. Lodato & Rice 2004), as seen in the theoretical predictions for HL Tau made by Greaves et al. (2008). Third, HL Tau is in an early phase of star formation (Class I evolving to Class II), emitting a 100-200 km/s highly collimated jet (Mundt et al. 1990). The ongoing accretion from the envelope means that the disc is likely relatively thick, massive and hot, yet the clarity of the gaps are more reminiscent of those found in sim-

ulations of thin, cold discs (e.g. our most successful attempt to reproduce the gaps in gas-only discs required $H/R \lesssim 0.02$).

This begs the question of whether the gaps seen in HL Tau are genuine signatures of planet formation, or due to some other phenomena such as clumping (Lyra & Kuchner 2013), magnetic or Rossby-wave instabilities (Pinilla et al. 2012) or condensation fronts (Zhang et al. 2015). Then again, the observation that the first four dark rings are located close to what would be resonances between planets orbiting in those locations, together with slight eccentricity observed in the rings are evidence in favour of carving by planets (Wolf et al. 2002; ALMA Partnership 2015).

Key is that the emission seen at the wavelengths observed by ALMA is from dust rather than gas. Dust grains settle and migrate in protoplanetary discs at a rate determined by the Stokes number, $S_{\rm t}$, the ratio of the stopping time to the orbital timescale (Weidenschilling 1977; Takeuchi & Lin 2002) with the stopping time depending on the grain size and gas density (Eq. 1). If mm-grains have settled to the mid-plane in HL Tau then the gap-carving seen by ALMA could be that induced in the thin dust disc rather than the relatively thicker gas disc, since it is easier to carve gaps in the dust (Paardekooper & Mellema 2004). The absence of spiral structure may also be explained by the dust. Simulations of dust grains near gaps carved by planets (Paardekooper & Mellema 2004, 2006; Maddison et al. 2007; Fouchet et al. 2007, 2010; Ayliffe et al. 2012) have demonstrated that dust grains close to $S_{\rm t} = 1$ form axisymmetric rings, with smaller dust grains more closely following the gas and larger grains trapped in resonances (Ayliffe et al. 2012).

Whether embedded planets in dusty gas discs can explain the axisymmetric gaps in HL Tau is the focus of this Letter.

⋆ giovanni.dipierro@unimi.it
† daniel.price@monash.edu

2   METHODS

2.1   Dust/gas simulations

We perform 3D global simulations of dust/gas discs with embedded protoplanets using the PHANTOM smoothed particle hydrodynamics (SPH) code written by DP (Price & Federrath 2010; Lodato & Price 2010; Price 2012; Nixon, King & Price 2013).

We assume a single grain size per calculation. For grains of mm-size and larger we employ the two fluid algorithm described in Laibe & Price (2012a,b). For calculations with smaller grains we employ our new single fluid algorithm based on the terminal velocity approximation (Laibe & Price 2014; Price & Laibe 2015). This algorithm has been extensively benchmarked on simple test problems including waves and shocks in dust/gas mixtures (Laibe & Price 2011, 2012a; Price & Laibe 2015), but this is our first application to planet formation, allowing us to evolve both small and large grains efficiently.

2.1.1   Drag prescription

We assume a physical drag prescription where the drag regime is chosen automatically depending on the ratio of the grain size to the gas mean free path (Kwok 1975; Paardekooper & Mellema 2006; Laibe & Price 2012b). All of the grain sizes used in this paper fall into the Epstein regime, meaning that the stopping time is given by

$$t_s = \frac{\rho_{grain} s_{grain}}{\rho c_s f} \sqrt{\frac{\pi \gamma}{8}}, \tag{1}$$

where ρ_{grain} is the intrinsic grain density (we assume 1 g/cm^3), s_{grain} is the grain size, $\rho = \rho_g + \rho_d$ is the total density of the mixture, c_s is the sound speed, $\gamma = 1$ is the adiabatic index and f is a correction factor for supersonic drag given by (Kwok 1975)

$$f \equiv \sqrt{1 + \frac{9\pi}{128} \frac{\Delta v^2}{c_s^2}}, \tag{2}$$

where $\Delta v \equiv \boldsymbol{v}_d - \boldsymbol{v}_g$ is the drift velocity between the dust and gas. Hence, the Stokes number $S_t \equiv t_s \Omega$ in the mid-plane is

$$S_t = 1 \left(\frac{\Sigma}{0.2\text{g/cm}^2} \right)^{-1} \left(\frac{\rho_{grain}}{3\text{g/cm}^3} \right) \left(\frac{s_{grain}}{1\text{mm}} \right) \left(\frac{f}{1} \right)^{-1}. \tag{3}$$

A caveat to the above drag prescription is that it assumes spherical grains. Fractal grain shapes or similar would change the effective Stokes number associated with a particular grain size.

2.1.2   Sink particles

We place three planets, initially located at 13.2, 32.3 and 68.8 au, in the three main gaps observed in HL Tau (ALMA Partnership 2015). We represent the protoplanetary bodies and the central star using sink particles (Bate, Bonnell & Price 1995) with accretion radii of 0.25, 0.25 and 0.75 au, respectively. Dust and gas can be accreted onto the sinks provided that the material is bound to the sink and the velocity divergence is negative. The planets are free to migrate due to planet-disc interactions and the viscous disc evolution. We found migration to be negligible on the timescales simulated.

2.2   Initial conditions

2.2.1   Gas

We set up the discs in PHANTOM using the standard procedure outlined in Lodato & Price (2010). The system comprises a cen-
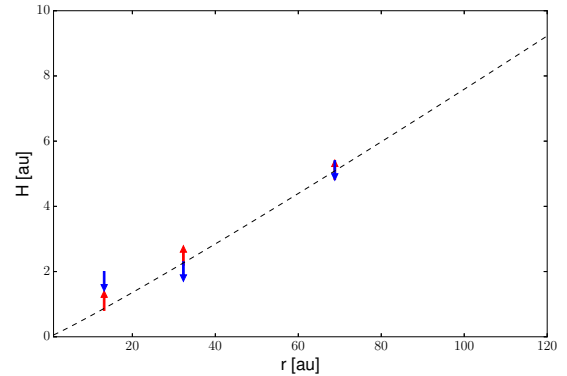

Figure 1. Constraint on the disc scale height profile obtained from the gap widths observed in the ALMA image (upper limits; blue points) combined with the lower limit obtained from the dust temperature as a function of radius (red points) along with our best fit $T \propto R^{-0.7}$ (dashed line).

tral star with mass $1.3M_\odot$ surrounded by a gaseous disc of 10^6 SPH particles which extends from $R_{in} = 1$ to $R_{out} = 120$ au. We assume a power-law surface density profile given by $\Sigma(R) = \Sigma_{in}(R/R_{in})^{-p}$, where Σ_{in} is the surface density at the inner edge. We assume a radially isothermal equation of state $P = c_s^2(R)\rho$, where $c_s = c_{s,in}(R/R_{in})^{-q}$, such that the gas temperature power law is $T(R) \propto (R/R_{in})^{-2q}$ and where $c_{s,in}$ is the sound speed at R_{in}. The aspect ratio in the gas is thus prescribed by the p and q indices according to $H/R = (H/R)_{in} (R/R_{in})^{\frac{1}{2} - q}$. We set the SPH α_{AV} viscosity parameter to 0.1 giving an effective Shakura & Sunyaev (1973) viscosity $\alpha_{SS} \approx 0.005$.

2.2.2   Constraining the disc model from HL Tau

While Kwon et al. (2011) fit various disc profiles to their previous low-resolution observations of HL Tau to constrain the surface density and temperature profiles, we use the gaps observed in the disc (ALMA Partnership 2015) to directly constrain the aspect ratio.

In particular, while the gap is deeper in the dust (Fouchet et al. 2007), the *width* is the same. Since a gap cannot be opened with a width less than the disc scale height the three prominent gaps observed in HL Tau provide an upper limit on H as a function of radius. Combining this with the dust temperature profile observed by ALMA, which, assuming that the dust and gas are thermally coupled, provides a lower limit on the gas temperature, we can directly constrain the sound speed profile. Figure 1 shows the constraint provided by the gap widths together with the lower limit and our best fitting power law $q = 0.35$ ($T \propto R^{-0.7}$) with $(H/R)_{in} = 0.04$. This gives $(H/R)_{out} \approx 0.08$.

We choose a shallow surface density profile $p = 0.1$ for computational efficiency since it avoids expensive computation of many particles on the shortest orbits. This reproduces the inner disc in our simulations, but gives an outer disc that is over-luminous compared to the inner disc in the simulated observations (Fig. 4). While more work is needed on the disc model, our main aim in the present paper is to reproduce the axisymmetry and size of the gaps.

2.2.3   Gas disc mass and dust-to-gas ratio

Hayashi et al. (1993) found a H$_2$ gas mass of $0.03M_\odot$ contained within 1400 au in HL Tau based on the observed ^{13}CO emission.
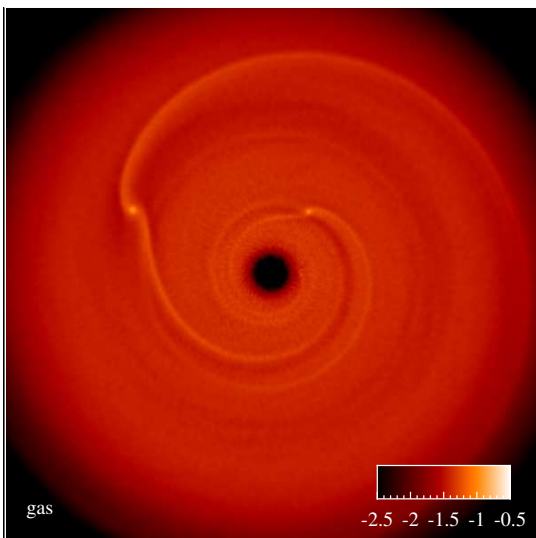
Figure 2. Rendered image of gas surface density for a disc containing three embedded protoplanets of mass 0.2, 0.27 and 0.55 M_J initially located at the same distance as the gaps detected in HLTau, at 13.2, 32.3 and 68.8 au.

We assume this as our starting point, noting the the mass contained with a particular radius depends on the density profile according to

$$M(< R) = \frac{2\pi}{2-p}\Sigma_{\rm in}R_{\rm in}^2 \left[\left(\frac{R}{R_{\rm in}} \right)^{2-p} - 1 \right]. \tag{4}$$

We assume the dust was initially co-located with the gas but has migrated to a radius ≈ 10 times smaller than the initial radius to give the 120 au dust disc visible with ALMA. Assuming an initial dust-to-gas ratio of 0.01 in the undifferentiated material at 1400 au, this gives $\Sigma_{\rm gas} \approx \Sigma_{\rm dust}$ within the smaller radius given our assumed p index of 0.1. Hence we assume a dust-to-gas ratio of unity within 120 au and set $\Sigma_{\rm in}$ such that $M_{\rm disc} = 0.03 M_\odot$ at 1400 au. The total gas mass within 120 au is thus 0.0002 $M_\odot$, but this is low mainly due to our assumed shallow surface density profile.

A steeper surface density profile, e.g. $p = 1$ would give a more realistic gas mass of $0.003 M_\odot$. While even this may seem in conflict with earlier fits to much higher disc masses (e.g. Robitaille et al. 2007; Kwon et al. 2011, 2015), these assume that the dust is co-located with the gas, whereas we expect settling and radial inward migration to produce a more compact dust disc, consistent with observations in other systems (Andrews et al. 2012; de Gregorio-Monsalvo et al. 2013). Moreover, Tamayo et al. (2015) found that such a massive gas disc within 120 au would smear out the eccentric features observed in HL Tau since the precession periods of pericentres would be faster than the timescale on which planets carve gaps. Our lower disc mass also ensures that the mm grains are close to $S_t = 1$ in order to guarantee an efficient migration towards the pressure maxima in the disc induced by the embedded protoplanets. Again, a steeper surface density profile would produce less coupling of the mm grains in the outer disc, giving dynamics similar to those we find with cm grains. Indeed, as we shall see, the spiral waves induced in larger grains by the outer planet do appear to be visible at mm wavelengths in HL Tau.

2.2.4 Dust

The dust disc is setup assuming an initially constant dust-to-gas ratio (equal to unity, see above). Since we simulate one grain size

at a time we assume a power-law grain size distribution given by

$$n(s) \propto s^{-m} \quad \text{for} \quad s_{\rm min} < s < s_{\rm max}, \tag{5}$$

where we assume $s_{\rm min} = 1\mu$m, $s_{\rm max} = 10$cm and $m = 3.5$ and perform six different simulations using $s = 1\mu$m, 10μm, 100μm, 1mm, 1cm and 10cm, respectively (Fig. 3). The grain size distribution is appropriate to interstellar dust and particles growing by agglomeration in protoplanetary discs (Draine 2006). While approximate, this is more realistic than assuming a constant dust-to-gas ratio for each grain size, capturing the main idea that small grains are more abundant than large grains.

In our two fluid simulations we set up the dust disc as a separate set of dust particles. We use one quarter of the number of dust particles compared to gas to prevent dust from becoming artificially trapped below the gas resolution (Laibe & Price 2012b; Ayliffe et al. 2012). For the calculations employing the single fluid algorithm (Price & Laibe 2015) there is only one set of particles describing the mixture, set up as described above for the gas but with a dust fraction ϵ set for each particle to provide an initially constant dust-to-gas ratio (i.e. $\epsilon = \rho_{\rm d}/\rho_{\rm g}/[1 + \rho_{\rm d}/\rho_{\rm g}]$). With both methods the dust is then free to settle and migrate in the disc, and feels gravity from both the central star and the embedded protoplanets.

2.3 Simulated ALMA observations

We perform simulated observations of our model using the RADMC-3D Monte Carlo radiative transfer code (Dullemond 2012) together with the Common Astronomy Software Application (CASA) ALMA simulator (version 4.1), focussing on ALMA band 6 (continuum emission at 233 GHz). The source is located in the position of HL Tau, adopting the disc inclination and position angle given by ALMA Partnership (2015). The procedure is as in Dipierro et al. (2015) except that the dust distribution is used directly from our simulation data rather than being prescribed. The dust model consists of spherical silicate grains with optical constant for magnesium-iron grains taken from the Jena database[1]. Full-resolution images produced by RADMC-3D simulations are used as input sky models to simulate realistic ALMA observations accounting for thermal noise from the receivers and the atmosphere and assuming a perfect calibration of the visibility measurements. A transit duration of 8 hours is used to reach an optimal signal-to-noise ratio. The observation parameters are chosen to match the spatial resolution of the observations (see caption of Fig. 4).

3 RESULTS

Fig. 2 shows the gas surface density, while Fig. 3 shows rendered images of the dust surface density from the disc model with three embedded protoplanets of masses of 0.2, 0.27 and 0.55 M_J, respectively, shown after $\sim$10 orbits of the outer planet. None of the planets produce clean gaps in the gas disc (Fig. 2), but as expected, the dust density perturbations induced by protoplanets depend strongly on the grain size (e.g. Fouchet et al. 2007; Ayliffe et al. 2012), or more specifically on the Stokes number. The density distribution of μm-sized particles (top left and centre) are similar to the gas distribution due to the stronger coupling. The micrometer sized grains

---

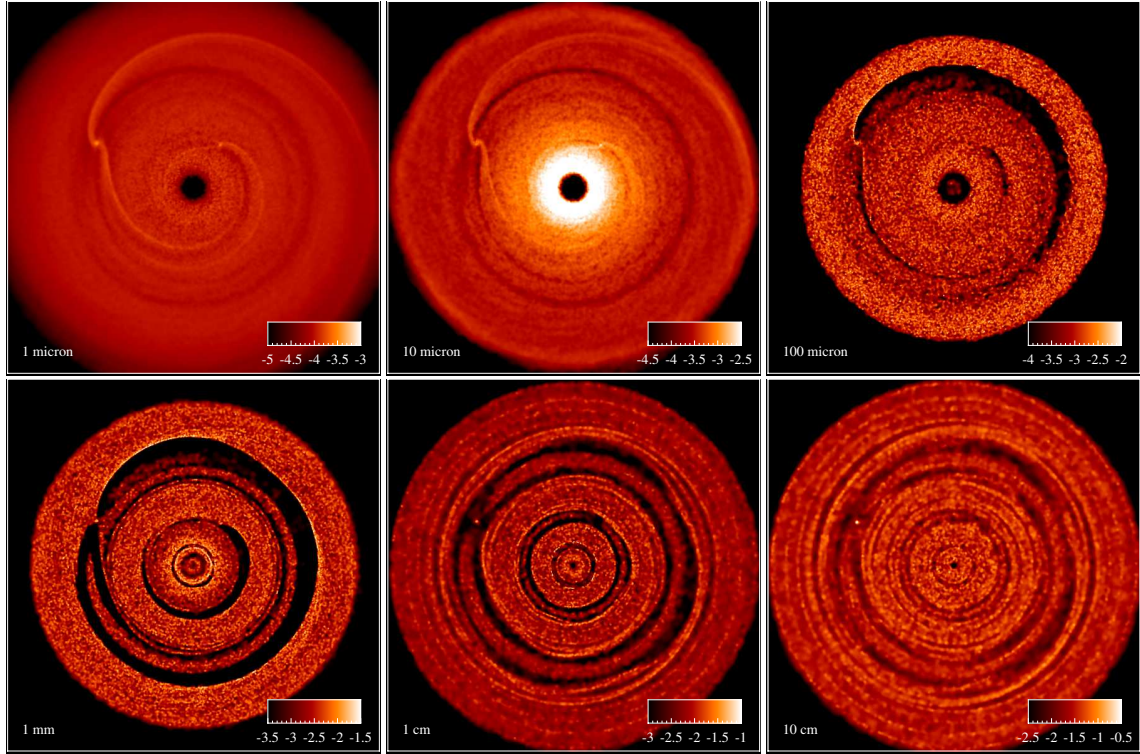[1] http://www.astro.uni-jena.de/Laboratory/Database/databases.html

Figure 3. Rendered images of dust surface density for a disc containing three embedded protoplanets of mass 0.2, 0.27 and 0.55 M_J initially located at the same distance as the gaps detected in HL Tau. Each panel shows the simulation with gas plus grains of a particular size (as indicated).

(top left) capture the spiral density wave launched by the protoplanets. Millimetre-sized particles (bottom left) are most affected by the density waves induced by the protoplanets, exhibiting the largest migration towards the gap edges. Interestingly, the dust density distributions of 10 mm and cm-sized particles (bottom centre and right) show axisymmetric waves launched by the planets propagating across the whole disc. The gaps carved by protoplanets in cm grains ($S_t \approx 10$) show the formation of horseshoe regions. As expected, the formation of the horseshoe region in planetary gaps depends on the dust-gas coupling, since poorly coupled large particles tend to have frequent close encounters with the planet. We stress that the important parameter is the Stokes number rather than the actual grain size, so equivalent dynamics can be produced in different grains by changing the gas density or with different assumptions about the grain composition (see Eq. 3).

An intriguing possibility is to infer the disc viscosity from the morphology of the gaps. Since our results show that the planets are not massive enough to open gaps in the gas or, equivalently, the viscosity is high enough to effectively smooth the density profile, we can only evaluate a lower limit for α_{SS} below which planets are able to carve gaps in the disc model adopted here. Using the criterion in Crida et al. (2006) we infer $\alpha_{SS} \gtrsim 0.0002$.

Fig. 4 compares the ALMA simulated observation of our disc model at band 6 (right) with the publicly released image of HL Tau (left). The pattern of bright and dark rings is readily detectable with ALMA using a selection of observation parameters that ensure a resolution close to the one reached in the real ALMA image. As expected, the emission probes the mid-plane disc surface density in large grains (0.1-10 mm), due to their high opacity at these wavelength (Dullemond et al. 2007; Williams & Cieza 2011). However, the intensity in the ALMA simulated observation of this model is lower than in the HL Tau image. This difference is likely due to the low dust mass, suggesting that the higher disc mass from a steeper surface density profile would produce better signal-to-noise ratio.

4 SUMMARY

Inspired by the recent ALMA image of HL Tau, we have performed 3D dust/gas SPH simulations of a disc hosting multiple planets aimed at reproducing the peculiar morphology of alternating dark and bright rings shown in the observation. We used 3D radiative transfer modelling to produce synthetic ALMA observations of our disc model in order to test whether dust features induced by embedded protoplanets can explain those detected. We find:

(i) The absence of spiral structure observed in HL Tau is due to the different response of the dust compared to the gas to embedded planets. Axisymmetric rings such as those observed are a natural product of embedded planets in the disc when observing the dust. Spiral structure may still be present in the gas. Hence dust/gas modelling is crucial for interpreting these systems.

(ii) In agreement with previous authors, we find it is easier to carve gaps in dust than in gas. Hence gaps observed in the continuum at mm-wavelengths do not necessarily indicate gaps in gas.

(iii) We can reproduce all the major features of HL Tau observations with three embedded planets at 13.2, 32.3 and 68.8 au with planet masses of 0.2, 0.27 and 0.55 M_J, respectively, though there is uncertainty in the exact masses from the assumed disc model. This supports the conclusion that embedded protoplanets are responsible. Our masses are similar to the 0.2 M_J suggested for all three planets in Dong et al. (2014) and consistent with a $10M_J$ upper limit for the third planet given by Testi et al. (2015).
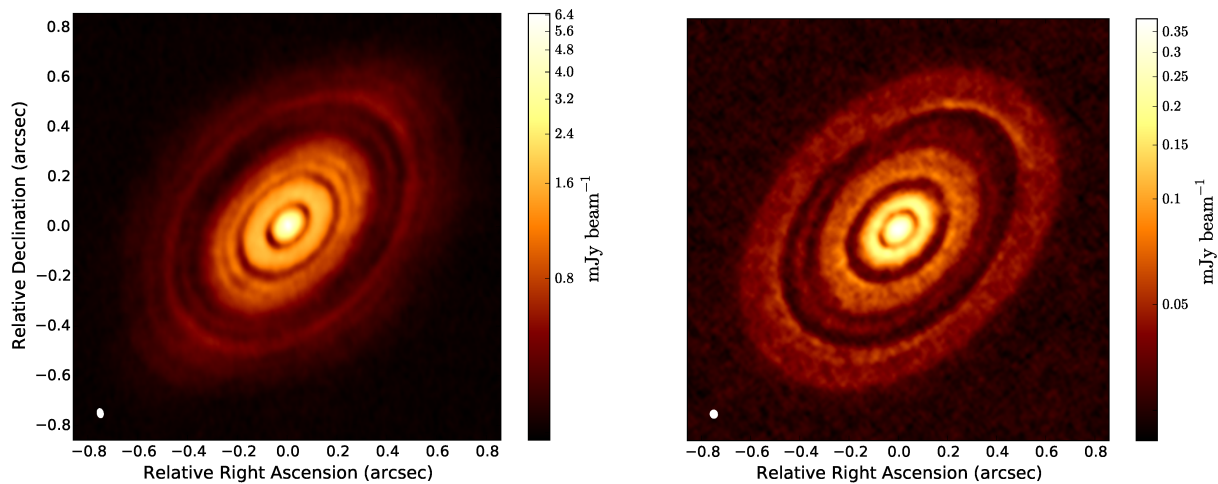
Figure 4. Comparison between the ALMA image of HL Tau (left) with simulated observations of our disc model (right) at band 6 (continuum emission at 233 GHz). Note that the color bars are different. The white colour in the filled ellipse in the lower left corner indicates the size of the half-power contour of the synthesized beam: (left) 0.035 arcsec × 0.022 arcsec, P.A. 11°; (right) 0.032 arcsec × 0.027 arcsec, P.A. 12°.

(iv) The dust density structures for grains with $S_t \gtrsim 10$ (cm-size and larger in our simulations; bottom centre and right panels of Fig. 3) show axisymmetric features that can be identified as waves excited by the embedded protoplanets (Goldreich & Tremaine 1980). These waves can freely propagate across the dusty disc without being damped by dissipative phenomena (Rafikov 2002). The lower drag makes these waves more visible since the drag effect on the radial dust motion is negligible. We therefore suggest that the axisymmetric perturbations in the ALMA images in the outer part of the second and third planet orbits are generated by the lower coupling of mm-particles. Further simulations with a steeper surface density profile should be able to reproduce this.

There are many caveats to our results, and these are preliminary investigations. Nevertheless they illustrate that the ALMA observations of HL Tau can be understood from the interaction between dust, gas and planets in the disc.

REFERENCES

ALMA Partnership 2015, arXiv:1503.02649,
Andrews S. M., et al., 2012, ApJ, 744, 162
Ayliffe B. A., Laibe G., Price D. J., Bate M. R., 2012, MNRAS, 423, 1450
Bate M. R., Bonnell I. A., Price N. M., 1995, MNRAS, 277, 362
Crida A., Morbidelli A., Masset F., 2006, Icarus, 181, 587
Dipierro G., Pinilla P., Lodato G., Testi L., 2015, MNRAS, 451, 5493
Dong R., Zhu Z., Whitney B., 2014, preprint, (arXiv:1411.6063)
Draine B. T., 2006, ApJ, 636, 1114
Dullemond C. P., 2012, RADMC-3D: A multi-purpose radiative transfer tool, Astrophysics Source Code Library (ascl:1202.015)
Dullemond C. P., et al., 2007, A&A, 473, 457
Fouchet L., et al., 2007, A&A, 474, 1037
Fouchet L., Gonzalez J.-F., Maddison S. T., 2010, A&A, 518, A16
Goldreich P., Tremaine S., 1980, ApJ, 241, 425
Greaves J. S., et al., 2008, MNRAS, 391, L74
Hayashi M., Ohashi N., Miyama S. M., 1993, ApJ, 418, L71
Kwok S., 1975, ApJ, 198, 583
Kwon W., Looney L. W., Mundy L. G., 2011, ApJ, 741, 3
Kwon W., et al., 2015, arXiv:1506.03679,
Laibe G., Price D. J., 2011, MNRAS, 418, 1491
Laibe G., Price D. J., 2012a, MNRAS, 420, 2345
Laibe G., Price D. J., 2012b, MNRAS, 420, 2365
Laibe G., Price D. J., 2014, MNRAS, 440, 2136
Lin D. N. C., Papaloizou J., 1986, ApJ, 307, 395
Lodato G., Price D. J., 2010, MNRAS, 405, 1212
Lodato G., Rice W. K. M., 2004, MNRAS, 351, 630
Lyra W., Kuchner M., 2013, Nature, 499, 184
Maddison S. T., Fouchet L., Gonzalez J.-F., 2007, Ap&SS, 311, 3
Mundt R., Buehrke T., Solf J., Ray T. P., Raga A. C., 1990, A&A, 232, 37
Nixon C., King A., Price D., 2013, MNRAS, 434, 1946
Paardekooper S.-J., Mellema G., 2004, A&A, 425, L9
Paardekooper S.-J., Mellema G., 2006, A&A, 453, 1129
Pinilla P., et al., 2012, A&A, 538, A114
Price D. J., 2012, J. Comp. Phys., 231, 759
Price D. J., Federrath C., 2010, MNRAS, 406, 1659
Price D. J., Laibe G., 2015, MNRAS, 451, 5332
Rafikov R. R., 2002, ApJ, 572, 566
Robitaille T. P., et al., 2007, ApJS, 169, 328
Shakura N. I., Sunyaev R. A., 1973, A&A, 24, 337
Takeuchi T., Lin D. N. C., 2002, ApJ, 581, 1344
Tamayo D., Triaud A. H. M. J., Menou K., Rein H., 2015, ApJ, 805, 100
Testi L., et al., 2015, ApJ, submitted
Weidenschilling S. J., 1977, MNRAS, 180, 57
Williams J. P., Cieza L. A., 2011, ARA&A, 49, 67
Wolf S., Gueth F., Henning T., Kley W., 2002, ApJ, 566, L97
Zhang K., Blake G. A., Bergin E. A., 2015, ApJ, 806, L7
de Gregorio-Monsalvo I., et al., 2013, A&A, 557, A133
de Val-Borro M., et al., 2006, MNRAS, 370, 529